



Deposited via The University of Sheffield.

White Rose Research Online URL for this paper:

<https://eprints.whiterose.ac.uk/id/eprint/90330/>

Version: Accepted Version

Article:

Gomez Sanz, S., McMillan, L., McGregor, J. et al. (2015) A new perspective on catalytic dehydrogenation of ethylbenzene: the influence of side-reactions on catalytic performance. *Catalysis Science and Technology*, 5 (7). pp. 3782-3797. ISSN: 2044-4753

<https://doi.org/10.1039/c5cy00457h>

Reuse

Items deposited in White Rose Research Online are protected by copyright, with all rights reserved unless indicated otherwise. They may be downloaded and/or printed for private study, or other acts as permitted by national copyright laws. The publisher or other rights holders may allow further reproduction and re-use of the full text version. This is indicated by the licence information on the White Rose Research Online record for the item.

Takedown

If you consider content in White Rose Research Online to be in breach of UK law, please notify us by emailing eprints@whiterose.ac.uk including the URL of the record and the reason for the withdrawal request.

A new perspective on catalytic dehydrogenation of ethylbenzene: the influence of side-reactions on catalytic performance

Sara Gomez ^a, Liam McMillan ^a, James McGregor ^{a,b*}, J. Axel Zeitler ^a, Nabil Al-Yassir ^d, Sulaiman Al-Khattaf ^d, Lynn F. Gladden ^a

^a University of Cambridge, Department of Chemical Engineering and Biotechnology, Cambridge CB2 3RA, UK

^b present address: University of Sheffield, Department of Chemical and Biological Engineering, Sheffield S1 3JD, UK

^d King Fahd University of Petroleum & Minerals, Dhahran 31261, Saudi Arabia

*james.mcgregor@sheffield.ac.uk

Abstract

The dehydrogenation of ethylbenzene to styrene is a highly important industrial reaction and the focus of significant research in order to optimise the selectivity to styrene and minimise catalyst deactivation. The reaction itself is a complex network of parallel and consecutive processes including cracking, steam-reforming and reverse water-gas shift (RWGS) in addition to dehydrogenation. The goal of this investigation is to decouple the major processes occurring and analyse how side-reactions affect both the equilibrium of ethylbenzene dehydrogenation and the surface chemistry of the catalyst. Studies have employed a $\text{CrO}_x/\text{Al}_2\text{O}_3$ catalyst and reactions have been conducted at 500, 600 and 700 °C. The catalyst and reaction have been investigated using elemental analysis, temperature programmed oxidation (TPO), temperature-programmed desorption (TPD), Raman spectroscopy, THz time-domain spectroscopy (THz-TDS), X-ray photoelectron spectroscopy (XPS), *in situ* infrared spectroscopy and on-line gas chromatography and mass spectrometry. The reaction profile shows an induction time corresponding to a cracking regime, followed by a dehydrogenation regime. The cracking period involves the activation of $\text{CrO}_x/\text{Al}_2\text{O}_3$ catalysts for dehydrogenation activity through a number of processes: cracking of ethylbenzene over acid sites; coke deposition; reduction of chromium from Cr (VI) to Cr (III); steam reforming activity over the reduced catalyst; and reverse water-gas shift reaction. Each of these processes plays a critical role in the observed catalytic activity. Notably, the presence of CO_2 evolved from the reduction of chromium by ethylbenzene and from the gasification of the deposited oxygen-functionalised coke results in the dehydrogenation reaction becoming partially oxidative, *i.e.* selectivity to styrene is enhanced by coupling of ethylbenzene dehydrogenation with the reverse water-gas shift reaction. Ethylbenzene cracking, coke gasification, steam-reforming and reverse water-gas-shift determine the relative quantities of CO_2 , CO, H_2 and H_2O and hence affect the coupling of the reactions. Coke deposition during the cracking period lowers the catalyst acidity and may contribute to chromium reduction, hence diminishing the competition between acid and metal sites and favouring dehydrogenation activity.

Keywords: Alumina-supported chromia; Ethylbenzene dehydrogenation; Styrene; Coke deposition.

1. Introduction

Catalytic dehydrogenation of ethylbenzene is the main industrial method to produce styrene^{1,2}, which is a precursor molecule for the synthesis of rubbers and plastics. In practice, the catalytic dehydrogenation process itself is part of a complex reaction network including not only dehydrogenation but also side-reactions. Atanda and co-workers employed a kinetic model to identify cracking as a major process that occurs simultaneously with dehydrogenation over hydrotalcite catalysts³, while other possible reactions can include reverse water-gas shift (RWGS), steam reforming of light hydrocarbons and the formation of hydrocarbonaceous deposits (“coke”). Coke is a major by-product which causes catalyst deactivation, although it can also act as the active species in oxidative dehydrogenation of ethylbenzene (ODH)^{4,5} and of light alkanes^{6,7} as well as in the direct dehydrogenation of *n*-butane⁸. Indeed carbon-based catalysts are widely employed in literature studies of ethylbenzene ODH⁹⁻¹¹. In the present work, CrO_x/Al₂O₃ is used as the catalyst for ethylbenzene dehydrogenation; this system enables the decoupling of the major reactions occurring, and as such it is possible to determine the role played by each process in influencing catalytic performance. A key parameter is the oxidation state of chromium, which is known to influence activity in dehydrogenation reactions of hydrocarbons such as propane¹². The motivation for the present study is to understand the relationship between side-reactions, catalyst surface composition (oxidation state) and catalytic activity, thereby facilitating the design of improved catalysts, and optimising process operating conditions.

In current industrial practice ethylbenzene dehydrogenation is typically performed in a fixed-bed reactor in the temperature range 540-650 °C and uses potassium-promoted iron (III) oxide mixed with additional promoters to stabilize the morphology of the catalyst or avoid sintering¹³⁻¹⁶. Although good ethylbenzene conversions are achieved with this system (60-65%)¹⁷ several challenges still remain. Ethylbenzene dehydrogenation is an endothermic reaction ($\Delta H = 129.4$ kJ/mol) and is limited by thermodynamic equilibrium, high excess of waste energy and deactivation of the catalyst by coke deposition resulting in loss of selectivity to styrene¹⁸. In order to minimise the formation of coke, maintain the correct oxidation state of the catalyst and enhance the reaction equilibrium, the reactor feed is usually diluted with steam,

hence increasing activity and selectivity¹⁹. At 600 °C and in the absence of steam, the equilibrium conversion is ~40%²⁰. However, if steam is added to the feed (steam/ethylbenzene: 20) or it is present in the gas phase, equilibrium conversion can achieve values up to 81%^{20,21}.

While Fe-based catalysts are widely used industrially, Cr-catalysts are also well-established materials for dehydrogenation of alkanes^{12,22,23} and may have benefits in oxidative dehydrogenation of ethylbenzene where CO₂ is used as the oxidant. For instance, Ye *et al.*²⁴ investigated the factors affecting the catalytic activity of CrO_x/Al₂O₃ for ethylbenzene dehydrogenation in the presence of CO₂. They also compared the catalytic performance of Cr₂O₃/Al₂O₃ with Fe₂O₃/Al₂O₃ catalysts. A conversion of 56% and a selectivity to styrene of 98.8% were achieved for a 20%Cr₂O₃/Al₂O₃ catalyst. In contrast, the conversion of ethylbenzene over a 20%Fe₂O₃/Al₂O₃ catalyst was 32.8% and the selectivity to styrene was 99.7%. These results showed that the chromia-based catalysts are more effective than the iron-based catalysts for ODH of ethylbenzene. In a different study²⁵, several modifiers (V, Ce, Co, Mn, Mo and Zn oxides) were used to improve Cr₂O₃/Al₂O₃ catalysts for ethylbenzene dehydrogenation with CO₂. Ce and V modified supported chromia catalysts showed enhanced conversion and selectivity to styrene (67.4% and 98.9%, respectively) as compared to the unmodified CrO_x/Al₂O₃ catalyst (57.5% and 99.0%). Other recent materials used for ODH of ethylbenzene with enhanced catalytic performance are mesoporous spinels (MAl₂O₄²⁶, Fe-doped MgAl₂O₄²⁷ and ternary iron-based catalysts (FeAlZn)²⁸). For instance, the spinel aluminates of Cu, Fe or Mg have been reported to be active towards styrene production and highly stable during the course of the reaction²⁶.

The objective of the present work is to establish an understanding of the various reactions and chemical species present in the reaction system and of their role in ethylbenzene dehydrogenation; no attempt has been made to develop an optimised catalyst. This investigation provides a scheme describing the interconnections between the different reactions and how they affect the surface chemistry and hence, the catalytic performance of the catalyst. To this end, alumina-supported chromia catalysts have been employed for ethylbenzene dehydrogenation. The catalytic tests were carried out in the temperature range 500-700 °C and over 1, 3 and 6 h time-on-

stream. The influence of reaction temperature and reaction time on the catalytic activity and selectivity of the catalysts were studied and the relationship of these parameters to the nature of carbonaceous deposits was investigated. Carbonaceous deposits formed on $\text{CrO}_x/\text{Al}_2\text{O}_3$ during ethylbenzene dehydrogenation were characterised by elemental analysis, temperature-programmed oxidation (TPO), Raman spectroscopy and terahertz time-domain spectroscopy (THz-TDS). In order to investigate the different reaction periods observed, several analyses were performed post-reaction, *e.g.* chromium oxidation state was probed by XPS; while the number and distribution of acid sites was characterised by NH_3 -temperature-programmed-desorption (NH_3 -TPD). In addition, catalytic tests over $\text{CrO}_x/\text{Al}_2\text{O}_3$ reduced in hydrogen prior to reaction, and $\text{CrO}_x/\text{Al}_2\text{O}_3$ pre-poisoned with 2,6-di-*tert*-butylpyridine (DTBP) were conducted to rationalise the role played by acid sites on the catalyst surface.

2. Experimental

2.1. Catalyst synthesis

Ethylbenzene dehydrogenation was carried out over an alumina-supported chromia catalyst with a chromium loading of 0.8 wt. %. This loading is significantly below monolayer coverage, *i.e.* where Cr_2O_3 crystals are first observed, which is achieved at a chromium loading of $\sim 12\%$ wt²⁹. Below monolayer coverage, the predominant surface chromium species are polymeric and monomeric Cr^{6+} ³⁰. In the present work the catalyst was prepared by wet impregnation using $\text{Cr}(\text{NO}_3)_3 \cdot 9 \text{H}_2\text{O}$ (Sigma-Aldrich, 99%) and the alumina support was $\gamma\text{-Al}_2\text{O}_3$ (Condea Chemie GmbH, Hamburg, Germany, BET surface area = $216 \text{ m}^2 \text{ g}^{-1}$). Approximately 15.98 g of $\text{Cr}(\text{NO}_3)_3 \cdot 9 \text{H}_2\text{O}$ and 20 g of $\gamma\text{-Al}_2\text{O}_3$ were added to 300 ml of water. The catalyst precursor was then mixed for 3 h at room temperature to ensure a homogeneous distribution of chromia on the support. After mixing, the solution was vacuum filtered and the filtrate was washed with water several times. The as-prepared solid was then dried in air at 393 K overnight and calcined for 24 h at 873 K, also in air. The color of the catalyst changed from green to yellow after calcination. Characterisation of the fresh catalyst by Raman spectroscopy showed bands in the $882\text{-}890 \text{ cm}^{-1}$ range corresponding to monochromate and polychromate species³¹.

2.2. Catalytic activity measurements

Ethylbenzene dehydrogenation was performed in a fixed-bed reactor connected to an on-line GC (Agilent 6890N Series, FID, column Agilent HP-5). Approximately 1 g of $\text{CrO}_x/\text{Al}_2\text{O}_3$ catalyst was placed in a fixed-bed reactor and pretreated under helium (1 barg, 40 ml min^{-1}) at $600 \text{ }^\circ\text{C}$ for 30 min. For the reaction studies, 40 ml/min of helium were flowed through a saturator filled with ethylbenzene at $70 \text{ }^\circ\text{C}$. The reactor was fed with 45 ml/min of a mixture of helium and ethylbenzene maintaining a He/EB ratio of 7.75 at atmospheric pressure. Gas chromatography measurements were taken every 20 min during a reaction time of 360 min. Conversion and selectivity to benzene, toluene, styrene and coke were determined according to Equations (1) and (2) and averaged over the steady state regime. It should be noted that conversion is calculated considering conversion to all products including coke. Selectivity to coke was calculated by applying a carbon mass balance as shown in Equation (3). After 6 h the catalyst was cooled down under 40 ml/min helium and removed for subsequent characterisation.

$$\text{conversion} = \frac{n_{\text{ethylbenzene,in}} - n_{\text{ethylbenzene,out}}}{n_{\text{ethylbenzene,in}}} \cdot 100 \quad (1)$$

$$\text{selectivity}_i = \frac{n_{i,\text{out}}}{n_{\text{benzene}} + n_{\text{toluene}} + n_{\text{styrene}} + n_{\text{methane}} + n_{\text{ethylene}} + n_{\text{coke}}} \cdot 100 \quad (2)$$

where i = benzene, toluene, styrene and coke

$$n_{\text{coke}} = n(C_{\text{ethylbenzene,in}}) - n(C_{\text{ethylbenzene,out}}) - n(C_{\text{productsout}}) \quad (3)$$

Reaction studies were also performed over a catalyst pre-exposed to 2,6-di-*tert*-butylpyridine (DTBP). DTBP selectively poisons Brønsted acid sites and hence this allows the contribution of such sites to the observed catalytic performance to be investigated. 1 g of catalyst was impregnated with 2 ml DTBP and held at $5 \text{ }^\circ\text{C}$ for 24 h. Samples were dried at ambient temperature for 12 h followed by further drying at $250 \text{ }^\circ\text{C}$ for 12 h. Ethylbenzene dehydrogenation was then performed over 1 g of pre-poisoned $\text{CrO}_x/\text{Al}_2\text{O}_3$ at $600 \text{ }^\circ\text{C}$ under identical conditions to the reaction over the

untreated catalyst. Additionally, the acid sites present were characterised by NH_3 -TPD at key times-on-stream as described in Section 2.3.

To investigate the influence of chromium oxidation state, experiments were conducted in which the catalyst was pre-reduced prior to reaction. Pre-reduction was carried out in a Catlab Microreactor module connected to an online quadrupole mass spectrometer (QIC-20, Hiden Analytical). 100 mg of catalyst was loaded and the temperature was increased from 50 to 550 °C (10 °C/min) under 20 ml/min of 5% H_2/He . The reduction temperature (550 °C) was chosen to coincide with the transition from Cr(VI) to Cr(III) established by TPR measurements (Section 3.2).

Ethylbenzene dehydrogenation over the pre-reduced catalyst was then carried out at 600 °C in the microreactor by flowing 20 ml/min through a saturator filled with ethylbenzene and heated to 70 °C ($\text{He}/\text{EB} = 15.5$). The reaction was performed for a period of 40 min.

Additionally, *in situ* diffuse reflectance infrared spectroscopy (DRIFTS) studies were conducted in order to monitor the evolution of the surface-retained species during reaction. Ethylbenzene dehydrogenation over $\text{CrO}_x/\text{Al}_2\text{O}_3$ was conducted using a Thermo Nicolet Nexus 670 equipped with a DRIFTS cell (Praying Mantis High Temperature reaction chamber with ZnS windows, HVC-DWI-2) and MCT detector. Approximately 70 mg of catalyst was loaded into the reaction cell and pretreated by flowing helium (20 ml/min) at 600 °C for 30 min. Subsequently, 20 ml/min of helium was used as carrier gas through a saturator filled with ethylbenzene and heated at 70 °C. The reaction was allowed to proceed for 100 min during which time spectra were continuously acquired (64 scans with a resolution of 4 cm^{-1}). The spectrum of the fresh $\text{CrO}_x/\text{Al}_2\text{O}_3$ was subtracted from the spectra measured during the reaction, hence the final spectra represent only the adsorbed species on the catalyst surface.

2.3. Characterisation techniques

TPR was carried out over the fresh $\text{CrO}_x/\text{Al}_2\text{O}_3$ to investigate the change in oxidation state with reduction temperature. Approximately 100 mg of catalyst was loaded into the Catlab microreactor. The catalyst was pre-treated by heating from 50 °C to 600 °C

at a rate of 10 °C/min under a flow of helium at 40 ml/min, and held at 600 °C for 30 min. Subsequently, the catalyst was cooled down to 50 °C at a rate of 10 °C/min under the same conditions. Following pre-treatment, a 5% H₂/He feed at a total flow of 40 ml/min was fed to the reactor and the temperature was increased from 50 °C to 900 °C at a rate of 10 °C/min. This analysis demonstrated that reduction of Cr(VI) to Cr(III) and Cr(II) occurred at 550 °C and 900 °C, respectively.

Temperature programmed techniques were also employed to characterise the coke deposited during reaction. TPO investigations of the reacted catalysts employed a gas mixture of composition 5% O₂/He at a total flow rate of 40 ml/min. The heating rate was 10 °C/min from 50 °C up to 875 °C. TPD was performed in the same equipment by heating the catalyst from 40 °C to 900 °C at a rate of 10 °C/min under a helium flow rate of 40 ml/min and held at this temperature for 50 min. After this period, the reactor was cooled down to room temperature at a rate of 20 °C/min, retaining the helium flow at 40 ml/min.

Additionally, the coke deposits formed during reaction were also investigated by elemental analysis, THz-TDS and Raman spectroscopy. Elemental analysis (Microanalytical Department, Department of Chemistry, University of Cambridge) yielded the percentages of carbon, hydrogen and nitrogen present in the catalysts post-reaction.

THz-TDS measurements were performed at 293 K using an experimental set-up described previously^{32,33}. Samples were prepared by mixing 50 mg of catalyst with 150 mg of polyethylene (Sigma-Aldrich) which is transparent to THz radiation. Pellets were formed by pressing the two materials into 13 mm diameter dies by using a pellet press (Specac, Orpington, UK) with a force of 20.0 kN for 2 min. Pure polyethylene pellets of 150 mg were also produced as a reference for THz-TDS measurements. The as-prepared samples were scanned ten times over a 30 ps time window giving a spectral resolution of 30 GHz. The time per scan was 18 s resulting in a total acquisition time of 3 min.

Raman spectroscopy experiments to characterise coke deposits were undertaken by placing the catalysts on a cover glass at room temperature. Spectra were acquired

using 748.81 nm laser excitation (3 mW) at 5 cm^{-1} spectral resolution (Raman Rxn1 System, Kaiser Optical Systems Inc., supplied by Clairet Scientific). Exposure time was 2 min and the laser power was set at 50 mW in order to minimise fluorescence/carbon oxidation effects. Both the fresh catalyst and empty sample holder spectra were recorded for background subtraction. The spectra were fitted by four components (G, D1, D3 and D4) and analysed in terms of positions, relative intensity and full width at half maximum amplitude (FWHM)³⁴⁻³⁶. Spectral analysis was performed considering Gaussian-shaped bands for D1, D3 and D4 bands and a Lorentzian-shaped for the G band. D2 was not considered in the study as this shoulder in the G band was not observed.

The morphological features of the fresh and coked $\text{CrO}_x/\text{Al}_2\text{O}_3$ catalyst after 6 h of ethylbenzene dehydrogenation were studied by high-resolution transmission electron microscopy (HRTEM). The measurements were performed by the Department of Materials Science and Metallurgy of the University of Cambridge by using a FEI Tecnai F20-G2 FEGTEM operated at 200 kV.

XPS of coked $\text{CrO}_x/\text{Al}_2\text{O}_3$ after ethylbenzene dehydrogenation was conducted in order to analyse the oxidation states of chromium. XPS measurements were performed on an Axis Ultra DLD (Kratos) with a monochromated Al- K_α X-ray source operated in electrostatic mode. The vacuum during analysis was *ca.* 1×10^{-8} mbar. Spectral analysis was carried out using CasaXPS software (Casa, <http://www.casaxps.com>, UK); both survey and narrow scan C1s and O1s spectra were obtained. Peaks were fitted using Gaussian curves against a linear background. Binding energies were fixed to previously established values, setting lower and upper bounds of ± 0.2 eV and leaving band widths as fitting parameters.

The influence of reaction and coke deposition on the number and distribution of acid sites was probed by NH_3 -TPD. These experiments were performed in the microreactor system described earlier. Approximately 100 mg of catalyst was pre-treated at 600 °C under 40 ml/min of helium for 30 min. Subsequently, adsorption of ammonia on the catalyst was conducted by flowing 40 ml/min of 5% NH_3/N_2 through the sample at 50 °C for 30 min to ensure saturation. After adsorption and in order to completely remove the physisorbed ammonia, 40 ml/min of helium was flowed for 1 h. Finally,

NH₃-TPD was carried out by increasing the temperature at 10 °C/min from 50 °C to 900 °C.

3. Results

3.1. Catalytic activity of fresh CrO_x/Al₂O₃

The dehydrogenation of ethylbenzene has been studied at three reaction temperatures (500, 600 and 700 °C). In all cases the reaction conditions result in a similar reaction profile (Fig. 1a), notably an initial period where activity is dominated by cracking to benzene, and to a lesser extent toluene, followed by a period in which a high steady-state selectivity towards styrene is obtained. The influence of reaction temperature on catalytic performance and coke formation is discussed in Section 3.1.1, while the effect of time-on-stream is discussed in Section 3.1.2. These data are used to examine the origins of the evolution of catalyst performance.

3.1.1. Effect of reaction temperature

A representative selectivity profile of the reaction at 600 °C *versus* time-on-stream is shown in Fig. 1b. During the initial cracking period (before 3 h time-on-stream), there is consecutive production of benzene followed by the formation of toluene. Styrene is only formed after 3 h time-on-stream (denoted as the dehydrogenation regime from hereon) and is associated with a decrease in selectivity to benzene and toluene; styrene formation rapidly reaches steady-state activity. Therefore, over this catalyst cracking and dehydrogenation occur sequentially with almost no cracking in the dehydrogenation regime; this enables the influence of cracking and dehydrogenation on catalyst structure and activity to be considered separately in contrast to previous studies where reactions occur concurrently^{3,37}. The steady state values of conversion and selectivity to benzene, toluene, styrene and coke were calculated and are reported in Table 1; conversion of ethylbenzene at 600 and 700 °C is ~100%. Selectivity to styrene is maximised at the intermediate temperature of 600 °C.

The coke deposited during ethylbenzene reaction at different reaction temperatures has been characterised by a variety of techniques, as follows.

Elemental analysis: Microanalysis conducted over the coked catalysts is shown in Table 2. The quantity of coke increases with reaction temperature, carbon comprising ~2 wt.% of the used catalyst at 500 °C, but ~24 wt.% at 700 °C. This increase in carbon-content of the coke with reaction temperature reflects the change in coke structure from more hydrogen-rich coke compounds at low reaction temperatures (500 and 600 °C) to more hydrogen-deficient coke residues at high reaction temperatures: at 700 °C the measured C/H ratio is 34:1. Note that the parameter %C_{coke} refers to the carbon content of the deposited coke (which is different to the percentage of the coke in the catalyst sample, %C) and is determined as follows:

$$\%C_{coke} = \frac{\%C}{\%C + \%H} \cdot 100 \quad (4)$$

The C/H mass ratio and %C_{coke} allow us to ascribe average molecular structures to the carbonaceous deposits. For instance, if the C/H mass ratio and %C_{coke} determined for coke deposits are 27.0 and 97.5, respectively, the average molecular structure would be similar to that of ovalene (C₃₂H₁₄). The evolution of coke with time-on-stream is discussed in Section 3.1.2.

TPO and THz-TDS: The influence of reaction temperature on the TPO and THz spectra of CrO_x/Al₂O₃ after ethylbenzene dehydrogenation is shown in Fig. 2a and Fig. 2b, respectively.

The TPO profile of CrO_x/Al₂O₃ reacted at 500 °C shows that coke is readily oxidized, with a small band appearing at ~ 420 °C (Fig. 2a). A larger band is observed for CrO_x/Al₂O₃ after reaction at 600 °C, with a slight change in the oxidation temperature (~ 450 °C). In contrast, at 700 °C, the magnitude of the peak height is significantly greater and the oxidation temperature is shifted to higher values (~ 550 °C). This confirms the conclusions of elemental analysis and shows that greater amounts of coke are deposited when increasing reaction temperature and a gradual change in coke structure takes place, from more amorphous coke at low reaction temperature (500-600 °C) to more graphitic-like structures at high reaction temperature (700 °C). Also, the change in oxidation temperature is more pronounced when the reaction temperature increases from 600 to 700 °C, which suggests a change in the nature of

coke towards more polyaromatic species, again in agreement with elemental analysis results.

THz spectra show the THz absorption coefficient of coked $\text{CrO}_x/\text{Al}_2\text{O}_3$ catalysts after ethylbenzene dehydrogenation at 500, 600 and 700 °C (Fig. 2b). Two temperature regimes can be distinguished: a low temperature regime (500-600 °C) characterised by low absorption coefficients (11.3 cm^{-1} at 500 °C and 17.1 cm^{-1} at 600 °C at 1 THz), and a high temperature regime (700 °C), for which a sudden increase in the magnitude of the absorption coefficient is observed (460 cm^{-1} at 1 THz). High THz absorption coefficients have been demonstrated to be attributed to high free-electron densities in extended networks with large regions of graphitic order and fewer terminations³³. Thus, the high absorption coefficient of $\text{CrO}_x/\text{Al}_2\text{O}_3$ coked at 700 °C indicates the presence of more extended domains of graphitic order.

Raman spectroscopy: The Raman spectra of the $\text{CrO}_x/\text{Al}_2\text{O}_3$ catalysts coked at 600 and 700 °C and the results of the fits are shown in Fig. 3 and Table 3, respectively. For the sample coked at 500 °C, the relatively low quantity of coke deposited resulted in the spectrum exhibiting a strong fluorescence background derived from the exposed Al_2O_3 support, and hence quantitative analysis of this spectrum was not possible. Fitting was performed by setting the positions of these bands according to the values reported in the literature for carbonaceous materials^{38,39} and establishing a boundary of $\pm 10 \text{ cm}^{-1}$. Values of FWHM were left as a free fitting parameter. The D1/G ratio has been traditionally used to characterise the degree of structural order of carbons⁴⁰⁻⁴². This ratio was employed for the first time by Tuinstra and Koenig⁴⁰ who related it to the crystallite size, L_a , obtained from X-ray diffraction. They observed a linear relationship between D1/G and $1/L_a$. However, it has been demonstrated that for D1/G ratios higher than 1.1 (amorphous carbons), this linear correlation is not valid⁴³. Since the values of D1/G are higher than 1.1 in the present work the D1/D3 ratios recorded are therefore taken as the primary indicator of the structural order of the coke present. The values of D1/G and D1/D3 ratios were calculated as the ratio of the peak areas obtained from the deconvolution of bands. The D1/G ratio is only slightly affected by reaction temperature, showing a lower value at 700 °C, which suggests an increase in structural organization of coke deposits. In contrast, reaction temperature significantly influences the D1/D3 ratio: this increases from 2.0 at 600 °C to 4.9 at 700 °C

reflecting that the structure changes from more disordered coke at 600 °C (mixture of paraffinic, olefinic, polyolefinic and alkyl aromatic coke compounds) to more ordered carbonaceous deposits (alkyl aromatic and polyaromatic coke species) at 700 °C. The presence of more ordered coke at 700 °C is associated with a higher selectivity to cracking products such as benzene (Table 1).

High-resolution transmission electron microscopy (HRTEM): Fig. 4 shows representative HRTEM images of fresh and coked $\text{CrO}_x/\text{Al}_2\text{O}_3$ after 6 h of ethylbenzene dehydrogenation at 600 °C. The poorly crystalline nature of the fresh catalyst is clearly observed (Fig. 4a) in accordance with the low resolution of the XRD diffraction lines. The d-spacing of the fresh catalyst is ~ 2.8 Å which corresponds with the (110) plane of $\gamma\text{-Al}_2\text{O}_3$ ^{44,45}. The catalyst coked at 600 °C (Fig. 4b) shows the presence of coke deposits. A detailed analysis showed that the C(002) spacing between lattice fringes ranges from 3.9 to 4.1 Å. As the d-spacing of the C(002) plane for graphite is ~ 3.34 Å⁴⁶, coke deposited after reaction at 600 °C can therefore be considered to be amorphous. The high values of the d-spacings for the coked $\text{CrO}_x/\text{Al}_2\text{O}_3$ are related to the presence of turbostratic aromatic coke structures as well as metastable carbon associated with the removal or formation of linkages during polymer carbonisation^{47,48}.

Taken together, the various analytical techniques confirm that a greater quantity of coke deposits are formed with increasing reaction temperature and that these deposits are more ordered. At this point, we note that a higher reaction temperature is also associated with a longer induction time during which cracking of ethylbenzene occurs before dehydrogenation predominates.

3.1.2. Effect of time-on-stream

As discussed in Section 3.1, Fig. 1b shows that catalytic behaviour varies as a function of time-on-stream with, *e.g.*, cracking and dehydrogenation regimes observed. This decoupling of different reactions allows us to probe the role each has on catalytic performance and on coke deposition. 600 °C has been selected as the reaction temperature for this study because it gives the clearest separation of the two regimes and has the highest selectivity to styrene of the three temperatures studied.

The times-on-stream studied are 1, 3 and 6 h. These correspond to: the maximum in benzene selectivity during the cracking regime; the maximum in styrene selectivity immediately after the transition point; and steady-state ethylbenzene dehydrogenation, respectively. Conversion of ethylbenzene at 600 °C increases from 16% at 1 h to 93% after 3 h, reaching 97% at 6 h. Selectivity to styrene increases during the cracking period from 0.8% (1 h) to 26% (3 h), decreasing to 15% at steady-state (6 h) (Fig. 1b).

Analysis of the coke deposited after 1, 3 and 6 h on-stream during ethylbenzene dehydrogenation at 600 °C was performed by different techniques. As shown in Table 4, elemental analysis indicates a linear increase in C/H ratio upon increasing the reaction time, from 2:1 after 1 h, to 10:1 after 6 h, suggesting a gradual condensation of coke species. These data show that 56% of the coke is deposited over the cracking period. NH₃-TPD, *vide infra* (Table 5), shows that the greatest contribution to “coke” during the dehydrogenation regime is the retention of aromatic products. The TPO results reported in Fig. 5 shows a gradual increase in the peak areas with time-on-stream, indicating that carbon deposition increases over the course of the reaction. The oxidation temperature remained approximately constant in the period 1-3 h on-stream (~ 444 °C) and slightly increased over the last 3 h of reaction (~ 454 °C), consistent with the presence of a more ordered coke structure after 6 h time-on-stream.

XPS was also conducted over the coked catalysts at different times-on-stream. Figure 4 shows the changes in surface composition of the chromium and carbon phases as a function of time-on-stream. Deconvolution of a typical C1s XPS spectrum of coked CrO_x/Al₂O₃ (Fig. 6a) allows quantification of oxygen functional groups and the proportion of functionalised and non-functionalised carbon. The atomic percentage of three types of oxygen functionalities was determined: i) electrophilic oxygen: carboxylic anhydrides and carboxylic acids, ii) neutral oxygen: ethers, lactones, phenols and iii) nucleophilic oxygen: ketones and quinones. Fig. 6b shows the C 1s/Al 2p and C 1s/Cr 2p ratios as a function of time-on-stream. A continuous increase in the carbon content relative to the chromium and alumina contents (C 1s/Al 2p and C 1s/Cr 2p, respectively) is observed for both cracking and dehydrogenation regimes. For instance, during the dehydrogenation period (3-6 h

time-on-stream) the C 1s/Cr 2p ratio changes from 1.0 to 1.7 and the C 1s/Al 2p ratio increases from ~0.6 to 1.0 due to the increase in the carbon content. The oxidation states of chromium were also analysed by deconvolution of the peaks present in the Cr 2p spectrum between 570 and 600 eV. Fig. 7a shows a typical Cr 2p spectrum of $\text{CrO}_x/\text{Al}_2\text{O}_3$ after 1 h of ethylbenzene dehydrogenation at 600 °C. The band appearing at ~576.5-576.7 eV is attributed to supported Cr^{3+} ; whereas binding energies for Cr^{6+} are expected to be found between 579.5 and 581 eV^{49,50}. The integration of the areas under the bands corresponding to Cr^{3+} and Cr^{6+} allowed the determination of the $\text{Cr}^{3+}/\text{Cr}^{6+}$ ratio of coked $\text{CrO}_x/\text{Al}_2\text{O}_3$ after 1, 3 and 6 h on-stream of ethylbenzene dehydrogenation at 600 °C. As seen in Fig. 7b, the $\text{Cr}^{3+}/\text{Cr}^{6+}$ ratio increases during the first 3 h of reaction (cracking period), which shows that Cr^{6+} undergoes reduction to Cr^{3+} . During the dehydrogenation regime (3-6 h on-stream), the $\text{Cr}^{3+}/\text{Cr}^{6+}$ ratio remained fairly constant and no Cr^{2+} was detected. Fig. 8 presents the selectivity profile for styrene as well as the atomic percentage of functionalised carbon with time-on-stream obtained from XPS analysis. Most of the carbon deposited after 6 h is non-functionalised $\text{sp}^2\text{-C}$ (15.3%), followed by 3.1% of carboxylic moieties and 1.5% of carbonyl groups. Small quantities of phenolic/ether groups are observed in the early period of reaction but are not observed after 1 h time-on-stream whereas carbonyl, carboxylic and non-functionalised $\text{sp}^2\text{-C}$ increase continuously with time-on-stream.

The number and distribution of acid sites on fresh and coked $\text{CrO}_x/\text{Al}_2\text{O}_3$ after 3 and 6 h of ethylbenzene dehydrogenation were studied by NH_3 -TPD. The data were fitted with Gaussian lineshapes; the peak position identifying the desorption temperature corresponding to different acid sites, classified according to their acid strength. The acid site distributions were classified by temperature range into weak or low energy acid sites (< 250 °C), medium energy acid sites (250-400 °C) and high energy acid sites (> 400 °C)⁵¹. Table 5 shows the number and distribution of acid sites of the fresh $\text{CrO}_x/\text{Al}_2\text{O}_3$ catalyst and after ethylbenzene dehydrogenation at 3 and 6 h time-on-stream determined by deconvolution of the NH_3 -TPD profiles. It is seen that during the cracking period the total number of acid sites decreased by only ~ 5 mmol NH_3/g as compared to the fresh catalyst. However, the decrease in total acidity over the dehydrogenation period (between 3 and 6 h time-on-stream) was ~ 18 mmol NH_3/g , which was attributed to retention of aromatics.

Evolution of carbon oxides was observed over the course of the reaction hence the oxygen content of coke was studied using TPD which is routinely employed for the characterisation of oxygen groups on carbon surfaces⁵². Oxygen groups present in carbon deposits can decompose into CO and CO₂ upon heating at different temperatures. The assignment of TPD peaks to the surface groups of carbon has been the subject of study in the literature^{53–56}. Table 6 shows the established decomposition temperatures of oxygenated functionalities on a carbon surface by TPD^{52,57}. TPD data for the catalysts coked after 1, 3 and 6 h of ethylbenzene dehydrogenation is presented in Fig. 9. The evolution of CO and CO₂ in the TPD spectra reflects that a greater overall quantity of oxygen functionalities is formed with increasing time-on-stream. A range of different functionalities is observed: the CO₂ band at 153 °C can be attributed to carboxylic acids; anhydrides are also present and they result in the peaks observed at 357 °C and 593 °C; carbonyl and/or quinones give rise to the CO band at ~900 °C. Over the first hour of reaction, carboxylic, anhydrides, phenols and carbonyl/quinones are formed in agreement with XPS data. Over the dehydrogenation period, oxygen functionalities become more heterogeneous as shown by the less pronounced CO₂-TPD profile recorded at 6 h (Fig. 9a). Carbonyl/quinone functionalities are continuously created during the 6 h of reaction as the CO-TPD profile shows (Fig. 9b); these observations are consistent with the XPS results presented in Fig. 6.

Finally, the coke species formed during ethylbenzene dehydrogenation over CrO_x/Al₂O₃ were analysed by *in situ* DRIFTS. Fig. 10 presents the infrared spectra of catalysts at different times-on-stream. It can be observed that after 1 min of reaction, some chemical species are already deposited on the catalyst surface. The bands located at 2330 cm⁻¹ and 2360 cm⁻¹ are due to carbon dioxide released into the gas phase. Simultaneously, bands located at 1530 cm⁻¹, 1430 cm⁻¹ and 1410 cm⁻¹ (ν_{as} (COO), ν_{s} (COO) and δ_{s} (CH₃)) reveal the presence of acetates/carboxylates⁵⁸. In addition, formate species bonded to the chromia and alumina phases are observed at 2970 cm⁻¹ and 2880 cm⁻¹ and at 3010 cm⁻¹ and 2930 cm⁻¹, respectively⁵⁹. Hydrocarbon-type surface species are also deposited from the beginning of the reaction. The bands located at 3070 cm⁻¹ and 1500 cm⁻¹ are due to unsaturated or aromatic species whereas the weak band at 2925 cm⁻¹ is attributed to aliphatic species. The ratio between aromatic and aliphatic coke compounds increases with time-on-

stream coupling with a higher C/H ratio at longer reaction times. The band located at 1590 cm^{-1} can be attributed to quinone-type structures^{39,58} which continuously form with time-on-stream supporting the TPD and XPS results.

3.2. Effect of pre-reduction of catalyst

Pre-reduction of the catalyst in H_2 was conducted at 550 and 900 °C in order to determine the influence of chromium oxidation state on the observed reaction profile. TPR analysis indicates that these temperatures correspond to reduction of Cr(VI) to Cr(III) and Cr(II) respectively. The ethylbenzene dehydrogenation reaction was conducted in a microreactor over the fresh catalyst (Fig. 11a,b), the $\text{CrO}_x/\text{Al}_2\text{O}_3$ catalyst reduced at 550 °C (Fig. 12a,b) and at 900 °C (Fig. 12c,d). The lower temperature reduction at 550 °C is, from the TPR data, expected to reduce the surface chromia species to Cr(III). A similar reaction profile to that obtained for the unreduced catalyst (Fig. 1b) is obtained indicating that pre-reduction at this temperature does not fully remove the induction time prior to the onset of dehydrogenation. The catalyst reduced at 900 °C shows negligible dehydrogenation activity, after an initial cracking period. Based on TPR results this is ascribed to the formation of Cr(II) which is known to be inactive towards dehydrogenation^{22,60–62}.

In addition, these microreactor studies provide insights into the additional side-reactions that occur during ethylbenzene dehydrogenation. Analysis of the gas-phase products by mass-spectrometry revealed the release of CO and CO_2 during the cracking period, and to a lesser extent in the dehydrogenation regime, coupled with the consumption of water (Fig. 11b). The formation of these gases occurs as a consequence of chromium reduction by ethylbenzene and steam reforming, dealkylation and steam dealkylation of ethylbenzene and toluene. Methane is produced mainly as a co-product of ethylbenzene hydrogenolysis into toluene and from CO methanation. Furthermore, a simultaneous release of CO and CH_4 , coupling with a decrease in styrene formation is observed (Fig. 11a,b). This demonstrates the competition between, on the one hand, ethylbenzene steam reforming and CO methanation and, on the other hand, ethylbenzene dehydrogenation. Since the ethylbenzene conversion at steady-state (97%, Table 2) is higher than the equilibrium

conversion for the non-oxidative dehydrogenation in steam (81%,^{20,21}) the data suggest that CO₂ is playing a role in shifting the equilibrium towards styrene through RWGS and that this coincides with the onset of dehydrogenation activity.

3.3. Influence of carbon laydown

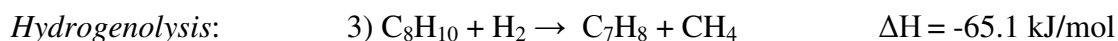
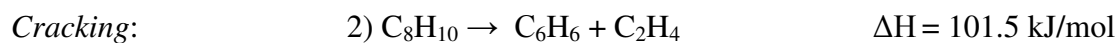
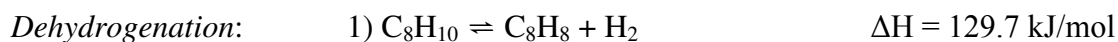
The quantity and nature of the carbon deposits, as described in Section 3.1, may exert a significant influence over the reaction. Elemental analysis (Table 4) shows that 56% of coke is deposited during the cracking regime. Cracking is an acid catalysed reaction and hence this coke can be assumed to form, initially, on acid sites. In order to distinguish the possible other effects of carbon deposition from the loss of Brønsted acid sites, studies have been carried out over CrO_x/Al₂O₃ poisoned with DTBP which selectively adsorbs on Brønsted acid sites⁶³⁻⁶⁵. The induction time prior to the onset of the dehydrogenation regime over the poisoned catalyst was still present and was shortened by only 20 min. Cracking and RWGS activity were still observed at short times-on-stream, however cracking activity was lower over the poisoned catalyst than the fresh material. Removing Brønsted acid sites alone does not result in higher activity towards ethylbenzene dehydrogenation, hence the origin of the cracking-dehydrogenation transition is not simply due to deactivation of more active, less selective, catalytic sites. Additionally, as was shown in Section 3.2, the transition is also not simply due to the reduction of Cr(VI) to Cr(III) during reaction. Note that coke species are considered unlikely to be the main species responsible for reduction of chromium, instead ethylbenzene and hydrogen are likely to be the main reducing agents. Similar conclusions have been drawn previously from propane dehydrogenation studies³⁷.

4. Discussion

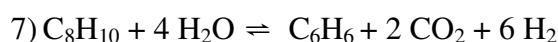
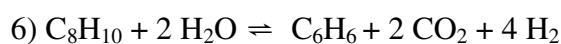
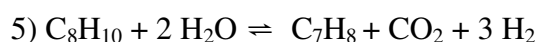
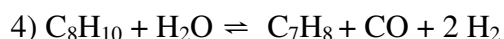
The reaction studies reported in Section 3 confirm that the ethylbenzene dehydrogenation reaction over CrO_x/Al₂O₃ in fact comprises a complex network of interdependent reactions. These are shown in Scheme 1:

Scheme 1. Reactions involved in ethylbenzene dehydrogenation

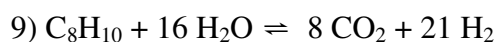
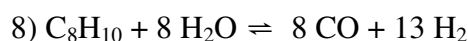
Reactions of ethylbenzene^{21,66}:



Steam reforming or dealkylation of ethylbenzene (endothermic):



Total steam reforming of ethylbenzene (endothermic):

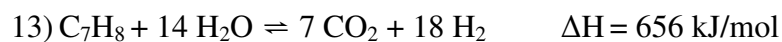
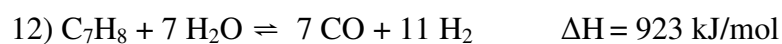


Reactions of toluene⁶⁷:

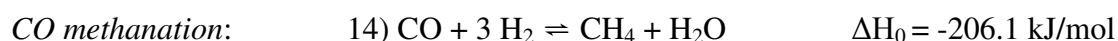
Steam reforming or dealkylation of toluene (endothermic):



Total steam reforming of toluene (endothermic):

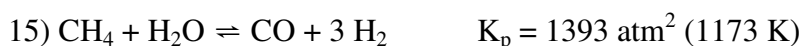


Reactions of CO⁶⁸:

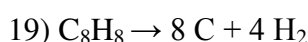
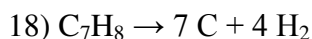
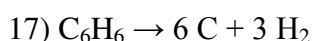
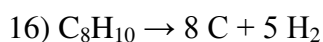


Reactions of methane⁶⁹:

Steam reforming of methane:



Coke formation (endothermic):

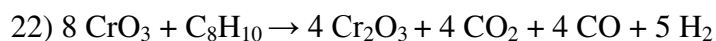
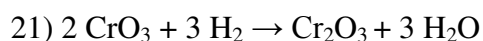


RWGS⁷⁰:



$$X_{\text{eq}} = 55\% (800 \text{ }^\circ\text{C})$$

Reduction of chromium:



While previous investigations have predominately focused on the dehydrogenation step, or in the case of oxidative dehydrogenation on its coupling with RWGS, we have attempted to further understand the role of each side-reaction (including coke formation) in determining overall catalytic behaviour. Each of these reactions has an influence on:

- *The surface chemistry of the catalyst; i.e., the ratio between acid and metal sites:* During the first stages of the reaction both cracking, steam reforming and coke deposition lead to the poisoning of acid sites. Therefore, these processes contribute to decreasing the competition between acid and metal sites available for dehydrogenation.
- *Thermodynamics of ethylbenzene dehydrogenation:* Ethylbenzene dehydrogenation is thermodynamically favoured by low partial pressures of hydrogen and additionally it can be coupled with RWGS. Thus, any side-reaction consuming hydrogen or releasing CO₂ has a positive effect on dehydrogenation activity. It is observed that steam reforming of toluene produces a higher proportion of H₂ relative to CO₂, hence it has a negative impact on the conversion of ethylbenzene. Steam reforming of methane lowers ethylbenzene conversion since it leads to a higher partial pressure of hydrogen. In addition, CO methanation is a coupling reaction with steam reforming of ethylbenzene, and these reactions

compete with ethylbenzene dehydrogenation. This is shown by the similar evolution of CO and CH₄ coinciding with the opposite trend in styrene formation (Fig. 11a,b)

- *Oxidation state of chromium:* the chromium oxidation state changes over the course of the reaction from Cr(VI) to Cr(III) mainly due to the contact between the metal sites and gaseous aromatic hydrocarbons. In addition, the presence of polyaromatic coke deposits may affect the reduction of chromium through hydrogen transfer reactions as has been reported in other studies ⁷¹. Further contact with gaseous aromatic hydrocarbons or coke deposition leads to the reduction from Cr(III) (active) to Cr (II)(inactive) which is a cause of catalyst deactivation, as seen after 360 min in the microreactor studies (Fig. 11a,b) .

Of particular note is the observation, discussed below, that CO₂ is released from reactions including the reduction of chromium oxide by ethylbenzene, steam reforming of hydrocarbons formed *in situ* ⁷² and from potential gasification of coke with evolved H₂O. The presence of CO₂ results in a partially oxidative reaction mechanism, even in the case of direct dehydrogenation where no additional oxidant is present in the reactant stream. This is demonstrated by the high values of ethylbenzene conversion at steady-state which are above the equilibrium value. For instance, the maximum of styrene selectivity at 600 °C (Fig. 1b, 180 min, 25%) may correspond to the equilibrium limit since ethylbenzene conversion (180 min, 78%) is close to the equilibrium conversion when steam is present (81%) ^{20,21}. Notice that at steady-state a supra-equilibrium conversion is achieved at 600 °C (97%, Table 1) which confirms that reaction coupling of ethylbenzene dehydrogenation with RWGS occurs ⁷³.

Detailed analysis of the results highlights the importance of side-reactions in influencing the surface and gas-phase concentrations of, in particular, CO, CO₂, H₂O and H₂. The concentration of these species is intimately related to the nature and quantity of the hydrocarbonaceous layer laid down on the catalyst surface. In turn this is related to the formulation of the catalyst and its operating conditions. The role of coke formation is not simply selective deactivation of acid sites: DTBP poisoning studies showed that this alone was not sufficient to remove the induction time prior to the onset of dehydrogenation. However, the generation of styrene does show a

correlation with the formation of coke. This can be ascribed to the fact that coke is not only a carbon sink but it also partakes in gasification/steam-reforming and reduction of the metal sites. Gasification of coke affects dehydrogenation activity in two competing ways: i) gasification “cleans” the catalyst resulting in a greater availability of acid sites for cracking, and hence the competition between dehydrogenation and cracking increases; ii) gasification of coke provides a second source of CO₂ (in addition to that released from chromium reduction) enhancing RWGS, and therefore dehydrogenation. The hydrocarbonaceous layer of coke may also influence chromium reduction through hydrogen reverse spillover as has been reported earlier for isopentane dehydrogenation⁷¹. Coke deposited over the surface of the support can abstract hydrogen from ethylbenzene and subsequently, hydrogen can be transferred to the metal causing chromium reduction.

The overall impact of the contrasting effects of coke formation on dehydrogenation activity depends upon the chemical nature of coke, *e.g.*, graphitic order and the stability of oxygen functionalities.

- More graphitic coke is less reactive towards gasification and less efficient at reducing chromium sites. In contrast, hydrogen-rich coke deposits participate in gasification and in chromium reduction through reverse spillover.
- The release of CO and CO₂ through RWGS and steam reforming causes the formation of oxygen functionalities on the coke surface (carboxylate, acetate, formate and carbonyl groups). These species have been reported to form in propane⁷² and isobutane⁵⁹ dehydrogenation through reduction of chromium by the alkane, and also from the reaction between gaseous hydrocarbons with surface hydroxyl groups. In addition, it has been claimed that carbonyl functionalities are the active species in oxidative dehydrogenation of ethylbenzene over activated carbons¹¹. However, in the present study no correlation between the changes in styrene selectivity and quantity of carbonyl groups can be identified (Fig. 8)

Deconvolution of the cracking and dehydrogenation regimes observed during ethylbenzene dehydrogenation allowed an understanding of the role of side-reactions, including steam reforming/dealkylation, RWGS and coke formation to be developed. All of these reactions affected the catalyst surface chemistry and the thermodynamics of ethylbenzene dehydrogenation. During the first stages of the reaction steam

reforming/dealkylation and cracking/coke deposition selectively poisoned the acid sites hence reducing the competition with metal sites. Thermodynamically, steam reforming of toluene and methane and CO methanation lowered ethylbenzene conversion through the increase in hydrogen partial pressure. Chromium was reduced readily by reaction between ethylbenzene with hydroxyl groups and through hydrogen-transfer from coke to the metal sites. Cr(III) was found to be the active species for dehydrogenation while further reduction of chromium to Cr(II) caused catalyst deactivation. Ethylbenzene conversion at steady-state was higher than the equilibrium conversion showing the positive role of CO₂ even when no additional oxidant was fed to the reactor. The main sources of CO₂ were chromium reduction by ethylbenzene and steam reforming of ethylbenzene and toluene. The inverse trends between CO, CH₄ and styrene over the dehydrogenation regime showed that ethylbenzene steam reforming and CO methanation are also coupling reactions, which explains the decrease in styrene selectivity (Fig. 11a,b). The nature of deposited coke changed from more disordered coke structures at low reaction temperatures (500-600 °C) to more ordered carbon networks at high reaction temperature (700 °C). The role of the carbonaceous layer is three-fold: to decrease the competition between acid and metal sites; to contribute to chromium reduction from Cr(VI) to Cr(III) and subsequently to Cr(II) causing catalyst deactivation; and to change the relative proportion CO/CO₂ through coke gasification hence affecting thermodynamics of ethylbenzene dehydrogenation.

5. Conclusions

TPO, TPD, Raman spectroscopy, THz-TDS, XPS, *in situ* infrared spectroscopy, and on-line gas chromatography and mass spectrometry have been used to characterise the surface of a CrO_x/Al₂O₃ catalyst during the ethylbenzene dehydrogenation reaction occurring at 500, 600 and 700 °C. At all temperatures the reaction profile shows an induction time corresponding to a cracking regime, followed by a dehydrogenation regime. The sequential nature of the cracking and dehydrogenation reactions, with almost no cracking in the dehydrogenation regime, enables the influence of cracking and dehydrogenation on catalyst structure, activity and selectivity to be considered separately. The cracking period involves the activation of CrO_x/Al₂O₃ catalysts for

dehydrogenation activity through a number of processes: cracking of ethylbenzene over acid sites; coke deposition; reduction of chromium from Cr(VI) to Cr(III); steam reforming activity over the reduced catalyst; and RWGS reaction. Each of these processes plays a critical role in the observed catalytic activity. Notably, the presence of CO₂ evolved from the reduction of chromium with ethylbenzene and from the gasification of the deposited oxygen-functionalised coke results in the dehydrogenation reaction becoming partially oxidative, *i.e.* selectivity to styrene is enhanced by coupling of ethylbenzene dehydrogenation with the reverse water-gas shift reaction. Ethylbenzene cracking, coke gasification, steam-reforming and reverse water-gas-shift determine the relative quantities of CO₂, CO, H₂ and H₂O and hence affect the coupling of the reactions. Coke deposition during the cracking period lowers the catalyst acidity and may contribute to chromium reduction, hence diminishing the competition between acid and metal sites and favouring dehydrogenation activity. Of the three reaction temperatures studied, selectivity to styrene is maximised at the intermediate temperature of 600 °C.

Acknowledgements

The authors express their appreciation to the support from the Ministry of Higher Education, Saudi Arabia, in establishment of the Center of Research Excellence in Petroleum Refining & Petrochemicals at King Fahd University of Petroleum & Minerals (KFUPM).

References

- 1 S. Carrà and L. Forni, *Ind. Eng. Chem. Process Des. Dev.*, 1965, **4**, 281–285.
- 2 G. Carja, R. Nakamura, T. Aida and H. Niiyama, *J. Catal.*, 2003, **218**, 104–110.
- 3 L. A. Atanda, N. O. Al-Yassir and S. Al-Khattaf, *Chem. Eng J.*, 2011, **171**, 1387–1398.
- 4 L. E. Cadus, L. A. Arrua, O. F. Gorrioz and J. B. Rivarola, *Ind. Eng. Chem. Res.*, 1988, **29**, 2241–2246.
- 5 L. E. Cadus, O. F. Gorrioz and J. B. Rivarola, *Ind. Eng. Chem. Res.*, 1990, **29**, 1143–1146.

- 6 T. G. Alkhozov, A. E. Lisovskii and Z. A. Talybova, *Neftekhimiya*, 1977, **17**, 687–689.
- 7 T. G. Alkhozov, A. E. Lisovskii, Y. A. Ismailov and A. I. Kozharov, *Kinet. Katal.*, 1978, **19**, 482–485.
- 8 J. McGregor, Z. Huang, E. P. J. Parrott, J. A. Zeitler, K. L. Nguyen, J. M. Rawson, A. Carley, T. W. Hansen, J.-P. Tessonnier, D. S. Su, D. Teschner, E. M. Vass, A. Knop-Gericke, R. Schlögl and L. F. Gladden, *J. Catal.*, 2010, **269**, 329–339.
- 9 M. Sugino, H. Shimada and T. Turuda, *Appl. Catal. A Gen.*, 1995, **121**, 125–137.
- 10 N. Keller, N. I. Maksimova, V. V. Roddatis, M. Schur, G. Mestl, Y. V. Butenko, V. L. Kuznetsov and R. Schlögl, *Angew. Chemie Int. Ed.*, 2002, **41**, 1885–1888.
- 11 M. F. R. Pereira, J. L. Figueiredo, J. J. M. Órfão, P. Serp, P. Kalck and Y. Kihn, *Carbon N. Y.*, 2004, **42**, 2807–2813.
- 12 O. F. Gorrioz, V. Cortés Corberán and J. L. G. Fierro, *Ind. Eng. Chem. Res.*, 1992, **31**, 2670–2674.
- 13 T. Hirano, *Appl. Catal.*, 1986, **28**, 119–132.
- 14 J.-N. Park, J. Noh, J.-S. Chang and S.-E. Park, *Catal. Letters*, 2000, **65**, 75–78.
- 15 T. Badstube, H. Papp, R. Dziembaj and P. Kustrowski, *Appl. Catal. A Gen.*, 2000, **204**, 153–165.
- 16 Z. Li and B. H. Shanks, *Appl. Catal. A Gen.*, 2011, **405**, 101–107.
- 17 C. Nederlof, PhD Thesis, Delft University of Technology, 2012.
- 18 D.-Y. Hong, V. P. Vislovskiy, Y.-H. Park and J.-S. Chang, *Bull. Korean Chem. Soc.*, 2006, **27**, 789–792.
- 19 N. Mimura and M. Saito, *Catal. Letters*, 1999, **58**, 59–62.
- 20 C. Hermann, P. Quicker and R. Dittmeyer, *J. Membr. Sci.*, 1997, **136**, 161–172.
- 21 H. S. Fogler, *Elements of Chemical Reaction Engineering*, Prentice-Hall, Englewood Cliffs, NJ, 1999.
- 22 F. Cavani, M. Koutyrev, F. Trifiró, A. Bartolini, D. Ghisletti, R. Iezzi, A. Santucci and G. Del Piero, *J. Catal.*, 1996, **158**, 236–250.
- 23 R. L. Puurunen and B. M. Weckhuysen, *J. Catal.*, 2002, **210**, 418–430.

- 24 X. Ye, W. Hua, Y. Yue, W. Dai, C. Miao, Z. Xie and Z. Gao, *New. J. Chem.*, 2004, **28**, 373–378.
- 25 X. Ye, Y. Yue, C. Miao, Z. Xie, W. Hua and Z. Gao, *Green Chem.*, 2005, **7**, 524–528.
- 26 A. H. de Moraes Batista, F. S. O. Ramos, T. P. Braga, C. L. Lima, F. F. de Sousa, E. D. B. Barros, J. M. Filho, A. S. de Oliveira, J. R. de Sousa, A. Valentini and A. C. Oliveira, *Appl. Catal. A Gen.*, 2010, **382**, 148–157.
- 27 M. Ji, X. Zhang, J. Wang and S.-E. Park, *J. Mol. Catal. A Chem.*, 2013, **371**, 36–41.
- 28 N. A. Ferreira, J. M. Filho and A. C. Oliveira, *RSC Adv.*, 2015, **5**, 20900–20913.
- 29 B. M. Weckhuysen and R. A. Schoonheydt, *Catal. Today*, 1999, **51**, 223–232.
- 30 S. De Rossi, M. P. Casaletto, G. Ferraris, A. Cimino and G. Minelli, *Appl. Catal., A Gen.*, 1998, **167**, 257–270.
- 31 M. Cherian, M. S. Rao, A. M. Hirt, I. E. Wachs and G. Deo, *J. Catal.*, 2002, **211**, 482–495.
- 32 P. C. Upadhyaya, K. L. Nguyen, Y. C. Shen, J. Obradovic, K. Fukushige, R. Griffiths, L. F. Gladden, A. G. Davies and E. H. Linfield, *Spectrosc. Lett.*, 2006, **39**, 215–224.
- 33 E. P. J. Parrott, J. A. Zeitler, J. McGregor, S.-P. Oei, H. E. Unalan, W. I. Milne, J.-P. Tessonnier, D. S. Su, R. Schlögl and L. F. Gladden, *Adv. Mater.*, 2009, **21**, 3953–3957.
- 34 R. J. Nemanich and S. A. Solin, *Phys. Rev. B*, 1979, **20**, 392–401.
- 35 J. Schwan, S. Ulrich, V. Batori and H. Ehrhardt, *J. Appl. Phys.*, 1996, **80**, 440–447.
- 36 M. A. Pimenta, G. Dresselhaus, M. S. Dresselhaus, L. G. Cançado, A. Jorio and R. Saito, *Phys. Chem. Chem. Phys.*, 2007, **9**, 1276–1291.
- 37 J. M. McNamara, S. David Jackson and D. Lennon, *Catal. Today*, 2003, **81**, 583–587.
- 38 O. Beyssac, B. Goffe, J.-P. Petit, E. Froigneux, M. Moreau and J.-N. Rouzaud, *Spectrochim. Acta, Part A*, 2003, **59A**, 2267–2276.
- 39 A. Sadezky, H. Muckenhuber, H. Grothe, R. Niessner and R. Pöschl, *Carbon N. Y.*, 2005, **43**, 1731–1742.
- 40 F. Tuinstra and J. L. Koenig, *J. Chem. Phys.*, 1970, **53**, 1126–1130.

- 41 Y. Wang, D. C. Alsmeyer and R. L. McCreery, *Chem. Mater.*, 1990, **2**, 557–563.
- 42 N. H. Cho, D. K. Veirs, J. W. Ager, M. D. Rubin, C. B. Hopper and D. B. Bogy, *J. Appl. Phys.*, 1992, **71**, 2243–2248.
- 43 S. Kumar, N. Kamaraju, B. Karthikeyan, M. Tondusson, E. Freysz and A. K. Sood, *J. Phys. Chem. C*, 2010, **114**, 12446–12450.
- 44 H. P. Rooksby, in *The X-ray identification and crystal structure of clay minerals*, ed. G. Brown, Mineralogical London Society, London, 1961, pp. 354–392.
- 45 Y. Repelin and E. Husson, *Mater. Res. Bull.*, 1990, **25**, 611–621.
- 46 K. Spyrou and P. Rudolf, in *Functionalization of graphene*, ed. V. Georgakilas, Wiley-VCH Verlag GmbH & Co., Weinheim, 2014, pp. 1–20.
- 47 F. J. M. Rietmeijer, *Carbon N. Y.*, 1991, **29**, 669–675.
- 48 J. Llorca, N. Homs, J. Sales and P. Ramírez de la Piscina, *J. Catal.*, 2002, **209**, 306–317.
- 49 R. Merryfield, M. McDaniel and J. Parks, *J. Catal.*, 1982, **77**, 348–359.
- 50 B. Grzybowska, J. Sloczynski, R. Grabowski, K. Wcislo, A. Kozłowska, J. Stoch and J. Zielinski, *J. Catal.*, 1998, **178**, 687–700.
- 51 V. Mohan, V. Venkateshwarlu, C. V. Pramod, B. D. Raju and K. S. R. Rao, *Catal. Sci. Technol.*, 2014, **4**, 1253–1259.
- 52 J. L. Figueiredo, M. F. R. Pereira, M. M. A. Freitas and J. J. F. Orfão, *Carbon N. Y.*, 1999, **37**, 1379–1389.
- 53 B. Marchon, J. Carrazza, H. Heinemann and G. A. Somorjai, *Carbon N. Y.*, 1988, **26**, 507–514.
- 54 Y. Otake and R. G. Jenkins, *Carbon N. Y.*, 1993, **31**, 109–121.
- 55 Q.-L. Zhuang, K. T. and A. Tomita, *Energy and Fuels*, 1994, **9**, 630–634.
- 56 U. Zielke, K. J. Huttinger and W. P. Hoffman, *Carbon N. Y.*, 1996, **34**, 983–998.
- 57 W. Shen, Z. Li and Y. Liu, *Recent Patents Chem. Eng.*, 2008, **1**, 27–40.
- 58 J. Coates, *Encycl. Anal. Chem.*, 2000, 10815–10837.
- 59 S. M. K. Airaksinen, M. A. Bañares and A. O. I. Krause, *Ind. Eng. Chem. Res.*, 2005, **44**, 3862–3868.

- 60 S. De Rossi, G. Ferraris, S. Fremiotti, E. Garrone, G. Ghiotti, M. C. Campa and V. Indovina, *J. Catal.*, 1994, **148**, 36–46.
- 61 A. Hakuli, A. Kytökivi, A. O. I. Krause and T. Suntola, *J. Catal.*, 1996, **161**, 393–400.
- 62 B. M. Weckhuysen, I. E. Wachs and R. A. Schoonheydt, *Chem. Rev.*, 1996, **96**, 3327–3349.
- 63 H. C. Brown and R. B. Johannesen, *J. Am. Chem. Soc.*, 1953, **75**, 16–20.
- 64 J. G. Santiesteban, J. C. Vartuli, S. Han, R. D. Bastian and C. D. Chang, *J. Catal.*, 1997, **168**, 431–441.
- 65 C. D. Baertsch, K. T. Komala, Y.-H. Chua and E. Iglesia, *J. Catal.*, 2002, **205**, 44–57.
- 66 W. J. Lee, PhD Thesis, Texas A&M University, 2005.
- 67 D. Duprez, *Appl. Catal. A Gen.*, 1992, **82**, 111–157.
- 68 J. Gao, C. Jia, M. Zhang, G. Fangna, G. Xu and F. Su, *Catal. Sci. Technol.*, 2013, **3**, 2009–2015.
- 69 J. M. Coulson, J. F. Richardson, J. R. Backhurst and J. H. Harker, *Chemical and Biochemical Reactors and Process Control*, Elsevier, Oxford, 1994.
- 70 S. Fujita, M. Usui and N. Takezawa, *J. Catal.*, 1992, **134**, 220–225.
- 71 K. Fujimoto and S. Toyoshi, in *7th Int. Cong. Catalysis*, 1981, p. 235.
- 72 S. Airaksinen and A. Krause, *J. Catal.*, 2005, **230**, 507–513.
- 73 D.-Y. Hong, V. P. Vislovskiy, S.-E. Park, M.-N. Park, J. N. Yoo and J.-S. Chang, *Bull. Korean Chem. Soc.*, 2005, **26**, 1743–1748.

List of Figure captions

Fig. 1. a) Conversion of ethylbenzene at 500 (◇), 600 (△) and 700 °C (□), and selectivity to styrene at 500 (◆), 600 (▲), and 700 °C (■) after ethylbenzene dehydrogenation over CrO_x/Al₂O₃ and b) conversion of ethylbenzene (△) and selectivity to toluene (▲), benzene (■) and styrene (◆) after ethylbenzene dehydrogenation over CrO_x/Al₂O₃ at 600 °C.

Fig. 2. a) Temperature-programmed oxidation of coked 0.8 wt. % CrO_x/Al₂O₃ after ethylbenzene dehydrogenation at 500, 600 and 700 °C after 6 h time-on-stream (40 ml/min, 5% O₂/He) and b) THz-TDS spectra of CrO_x/Al₂O₃ catalysts used in ethylbenzene dehydrogenation at 500, 600 and 700 °C.

Fig. 3. Raman spectra of CrO_x/Al₂O₃ after ethylbenzene dehydrogenation at a) 600 °C and b) 700 °C.

Fig. 4. High-resolution transmission electron microscopy (HRTEM) of a) fresh CrO_x/Al₂O₃ and b) coked CrO_x/Al₂O₃ after ethylbenzene dehydrogenation at 600 °C, 6 h time-on-stream.

Fig. 5. Temperature-programmed oxidation of coked CrO_x/Al₂O₃ after ethylbenzene dehydrogenation at 600 °C after 1, 3 and 6 h time-on-stream (40 ml/min, 5% O₂/He).

Fig. 6. a) C 1s XPS spectrum of coked CrO_x/Al₂O₃ during ethylbenzene dehydrogenation after 1 h time-on-stream, b) C 1s/Al 2p and C 1s/Cr 2p of coked CrO_x/Al₂O₃ after 1, 3 and 6 h time-on-stream.

Fig. 7. a) Cr 2p XPS spectrum of CrO_x/Al₂O₃ after 1 h of ethylbenzene dehydrogenation showing the bands attributed to Cr³⁺ and Cr⁶⁺ and b) Cr³⁺/Cr⁶⁺ ratios of CrO_x/Al₂O₃ after 1, 3 and 6 h on-stream of ethylbenzene dehydrogenation.

Fig. 8. Atomic percentages of functionalised carbon formed over CrO_x/Al₂O₃ during ethylbenzene dehydrogenation at 600 °C after 1, 3 and 6 h time-on-stream.

Fig. 9. a) CO₂-TPD spectrum of CrO_x/Al₂O₃ catalysts after ethylbenzene dehydrogenation for 1, 3 and 6 h time-on-stream and b) CO-TPD spectrum of CrO_x/Al₂O₃ catalysts after ethylbenzene dehydrogenation for 1, 3 and 6 h time-on-stream.

Fig. 10. DRIFTS spectra of *in-situ* ethylbenzene dehydrogenation over CrO_x/Al₂O₃ at 600 °C (flow of helium: 20 ml/min, He/EB: 7.75, mass of catalyst: 70 mg).

Fig. 11. Ethylbenzene dehydrogenation at 600 °C over fresh CrO_x/Al₂O₃ in a microreactor showing a) evolution of methane, toluene, benzene, ethylbenzene and styrene and b) evolution of the RWGS products.

Fig. 12. Ethylbenzene dehydrogenation at 600 °C over CrO_x/Al₂O₃ after pre-reduction at 550 °C (a,b) and 900 °C (c,d). Note that the timescales for the reactions over the fresh and reduced CrO_x/Al₂O₃ are different.

List of Table captions

Table 1. Conversion for ethylbenzene dehydrogenation over $\text{CrO}_x/\text{Al}_2\text{O}_3$ at 500, 600 and 700 °C after 6 h time-on-stream.

	Reaction temperature (°C)		
	500	600	700
Conversion (%)	79	97	99
Selectivity (%)			
benzene	0.09	1.3	1.4
toluene	0.6	2.9	2.5
styrene	2.2	15.1	4.0
methane	0.1	0.3	0.4
ethylene	0.2	0.3	0.4
coke	96.7	80.1	91.4

Table 2. Elemental microanalysis data showing the wt. % carbon and hydrogen and C/H mass ratio after 6 h time-on-stream over $\text{CrO}_x/\text{Al}_2\text{O}_3$ catalysts at 500, 600, 700 °C. % C_{coke} is calculated as $\% \text{C} / (\% \text{C} + \% \text{H}) \times 100$.

Temperature	%C (wt. %)	%H (wt. %)	C/H mass ratio	% C_{coke} (wt. %)
500 °C	1.9 ± 0.06	0.7 ± 0.05	2.7 ± 0.3	73.1 ± 1.90
600 °C	6.3 ± 0.17	0.6 ± 0.03	10.5 ± 0.7	91.3 ± 0.6
700 °C	23.5 ± 1.9	0.7 ± 0.04	33.6 ± 5.0	97.1 ± 0.40

Table 3. Position of the Raman bands, FWHM, D1/G and D1/D3 ratios of the Raman spectra of coked $\text{CrO}_x/\text{Al}_2\text{O}_3$ after ethylbenzene dehydrogenation at 600 °C and 700 °C.

		600 °C	700 °C
D4	Position (cm^{-1})	1200	1200
	FWHM	91	132
D1	Position (cm^{-1})	1363	1349
	FWHM	180	176
D3	Position (cm^{-1})	1520	1501
	FWHM	236	146
G	Position (cm^{-1})	1595	1596
	FWHM	116	100
Intensity ratios			
D1/G		1.8 ± 0.1	1.4 ± 0.1
D1/D3		2.0 ± 0.2	4.9 ± 0.3

Table 4. Elemental analysis data showing the wt. % carbon and hydrogen and C/H mass ratio after 1, 3 and 6 h time-on-stream over CrO_x/Al₂O₃ catalysts at 600 °C. % C_{coke} is calculated as %C / (%C+%H) × 100.

Time-on-stream (h)	%C (wt. %)	%H (wt. %)	C/H mass ratio	%C _{coke} (wt. %)
1	1.5 ± 0.008	0.7 ± 0.01	2.0 ± 1.8	67.0 ± 1.6
3	3.5 ± 0.03	0.6 ± 0.05	5.6 ± 0.8	84.8 ± 1.7
6	6.3 ± 0.20	0.6 ± 0.03	10.4 ± 1.0	91.2 ± 0.7

Table 5. Number and distribution of acid sites of the fresh CrO_x/Al₂O₃ catalyst and after ethylbenzene at 3 and 6 h time-on-stream as determined by NH₃-TPD.

Acidity (mmol NH ₃ /g)	Fresh CrO _x /Al ₂ O ₃	Coked CrO _x /Al ₂ O ₃ , 3 h	Coked CrO _x /Al ₂ O ₃ , 6 h
low strength	0.20	0.17	0.10
medium strength	0.19	0.21	0.12
high strength	0.10	0.07	0.04
total acidity	0.49	0.44	0.26

Table 6. Oxygen functionalities on carbon surfaces and their decomposition temperature by TPD

57

Oxygen functionality	TPD signal	Decomposition temperature (°C)
Anhydride	CO, CO ₂	350 °C - 627 °C
Carboxylic	CO ₂	100 °C - 400 °C
Carbonyl	CO	700 °C - 900 °C
Ether	CO	700 °C
Lactone	CO ₂	190 °C - 650 °C
Quinone	CO	700 °C - 980 °C
Phenol	CO	600 °C - 700 °C